

3.2 THE SHEAR CONTRIBUTION TO THE EVOLUTION OF A CONVECTIVE BOUNDARY LAYER

David Pino *

Institut d'Estudis Espacials de Catalunya (IEEC/CSIC), Barcelona, Spain

Peter G. Duynkerke

Institute for Marine and Atmospheric Research, Utrecht University, Utrecht, The Netherlands

Jordi Vilà-Guerau de Arellano

Meteorology and Air Quality Group, Wageningen University, Wageningen, The Netherlands

1. INTRODUCTION

Boundary layer growth is one of the main features in meteorology and air quality because it controls cloud formation and pollutant distribution. The growth of this convective boundary layer depends on two buoyancy mechanisms: surface fluxes of heat and moisture, and entrainment of dry air from the free atmosphere. The physics of this process can be substantially modified by wind shear (Schmidt and Schumann, 1989). Moreover, when both shear and buoyancy are important, the structure of the CBL flow is found to differ from the structure of either a purely mechanical boundary layer or a convective boundary layer. In the former case, the convection pattern is in the form of horizontal rolls (Christian and Wakimoto 1989).

In this work, on the basis of observations and large eddy simulations (LES), the role played by shear at the surface and inversion levels and its influence on the entrainment flux is discussed. The study stems from a specific situation that occurred on 20 June 1997 at the Southern Great Plains (SGP) Atmospheric Radiation Measurements (ARM) site where a convective boundary layer with high entrainment rates and increasingly strong horizontal winds was observed. Three CBLs with the same surface fluxes and initial profiles, except for the mean winds, were calculated by means of LES and the results were compared with the evolution of the observed CBL.

Specifically, we are interested in the processes that drive the entrainment flux. By working with LES it is possible to calculate the TKE budgets that let us to infer the importance of the contribution of the shear. Moreover, the TKE budget provided by LES allows us to verify the descriptions proposed in previous works. Following Driedonks (1982), the buoyancy flux ratio, $\beta = -\overline{w\theta_v}|_h/\overline{w\theta_v}|_0$, is selected for studying the entrainment processes. Current parameterizations for this ratio are tested by comparing it with the simulation results. On the basis of the intercomparison with LES results, a new expression for the buoyancy flux ratio which can be used in larger scale atmospheric models is proposed.

* Corresponding author address: David Pino, Institut d'Estudis Espacials de Catalunya (IEEC/CSIC), Edif. Nexus, Gran Capità 2-4, 08034 Barcelona, Spain; e-mail: pino@ieec.fcr.es.

2. OBSERVATIONS AND NUMERICAL SETUP

2.1 Observations

At the SGP site of the ARM program, located in Oklahoma and Kansas, various types of atmospheric measurements are monitored continuously by in-situ observations and remote sensing: vertical profiles of potential temperature, specific humidity and horizontal winds were measured each three hour from five different radiosondes; wind profiler measurements were taken to determine wind vertical profiles and mixing layer height. In addition, the surface sensible and latent fluxes, were estimated from observations using the Bowen ratio method.

During the day, clear skies were reported at all the sites. The synoptic situation is characterized by a low-level pressure system located west of the area studied which caused south-southwesterly winds and a decrease in the ground temperature towards the east. It is therefore, clear that during the day in question, the CBL development was influenced by shear at the surface and in the entrainment zone. Wind profile observations show the absence of subsidence motion during the analyzed day.

2.2 Numerical setup

Three different runs of the LES model described in Cuijpers and Duynkerke (1993) and recently modified by Cuijpers and Holtslag (1998) were performed for studying the evolution of the CBL during the 20 June 1997 at the SGP site. In the three simulations, all the initial and boundary conditions are identical except for the initial wind profile. The first case is defined as a boundary layer driven only by pure surface buoyancy, without geostrophic winds, namely B (buoyancy). The second and third cases, where geostrophic winds are introduced, consist of flows driven by both shear and buoyancy. In the former case (BG, buoyancy-geostrophic), the geostrophic wind is constant with height and the shear occurs only at the surface ($U_g = V_g = 10 \text{ m s}^{-1}$). In the latter, the initial wind profile corresponds approximately to the winds observed during that day ($U_g = 10 \text{ m s}^{-1}$ and $V_g = 17 \text{ m s}^{-1}$ for $z < 1000 \text{ m}$ and $U_g = V_g = 10 \text{ m s}^{-1}$ above this point). In this simulation the geostrophic shear also occurs near the inversion (BGS, buoyancy-geostrophic-sheared). A $6.4 \times 6.4 \times 3 \text{ km}^3$ domain with grid spacing $\Delta x = \Delta y = 100 \text{ m}$ and $\Delta z = 50 \text{ m}$ is defined. The total simulation time was 39600 seconds, i.e., the entire daily evolution.

As mentioned above, the same surface fluxes are considered in the three simulations. The maximum value of the surface sensible and latent heat fluxes for the simulations is obtained by adjusting a sinusoidal function to the average flux of the measurements of each facility. By so doing, the maximum values of the sensible and latent heat flux are $SH=120 \text{ W m}^{-2}$ and $LE=440 \text{ W m}^{-2}$.

The radiosonde at 14:30 UTC (LT=UTC-6) is used as the initial vertical profile of potential temperature ($\bar{\theta}$) and specific humidity (\bar{q}). The initial mean potential temperature (specific humidity) profile for all the simulations is 306 K (15.6 g kg^{-1}) below 625 m; it changes by 6 K (decreases 9.8 g kg^{-1}) up to 825 m, and increases until it reaches 317.8 K at 3 km (after this point, it has a constant value of 5.8 g kg^{-1}).

3. RESULTS

In this paper we only present, specifically, the contribution of shear to the evolution of the entrainment coefficient (β) and its parameterization. We therefore concentrate in analyzing the TKE budget. So doing we obtain an expression for the β parameter which only depends on observational meteorological variables. Previously, we show the comparison of LES and observations.

3.1 Potential temperature, specific humidity and mean winds

The comparison, for three different moments of the day (17:30, 20:30 and 23:30 UTC), of the vertical profiles of the potential temperature and specific humidity observed by the radiosondes and obtained with the B and BGS simulations (not displayed here) shows that both simulations agree well with the evolution and the vertical distribution of the CBL for a clear day. The calculated profiles follow very well the vertical profile evolution of the temperature and moisture observations. However, the BGS case fits better to the observations, in particular if the potential temperature is compared. In general, the B simulation tends to underestimate the inversion height. From the results, it is clear that a large entrainment situation occurs, where the mixing layer height grows from 703 m at 15 UTC to 1368 m at 20 UTC.

Fig. 1 shows the mean winds obtained by the various observational methods and the results of the simulation BGS around 20:30 UTC. As can be observed, there is a good agreement between the radiosonde at 20:30 UTC and the LES output averaged between 7 and 8 hours of simulation. Both profiles fit approximately in the middle of the data provided by the wind profiler located at the central facility. It is therefore possible, to include realistic profiles in the LES runs for obtaining the observed evolution of the atmospheric boundary layer.

3.2 Turbulent kinetic energy budget

Under horizontally homogeneous conditions and without subsidence, the turbulent kinetic energy budget

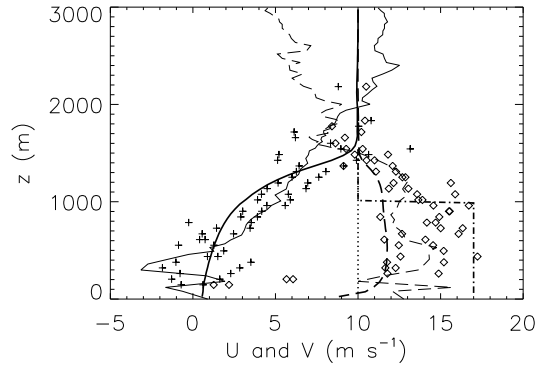


FIG. 1: Vertical profiles of mean winds. The radiosonde profiles obtained at the central facility of the SGP site at 20:30 UTC (U solid line, V dashed line) are shown with thin lines. The thick lines represent velocities integrated between 7–8 hours (U solid line, V dashed line), and the initial profile of the BGS simulation (U dotted line, V dashed–dotted line). Crosses and diamonds are, respectively, U and V velocity measured between 19 and 21 UTC by the wind profiler located at the central facility.

reads:

$$\frac{\partial \bar{e}}{\partial t} = - \left[\overline{uw} \frac{\partial U}{\partial z} + \overline{vw} \frac{\partial V}{\partial z} \right] + \frac{g}{\theta_v} \overline{w\theta_v} - \frac{\partial \overline{we}}{\partial z} - \frac{\partial \overline{wp/\rho_0}}{\partial z} - \epsilon, \quad (1)$$

where $\bar{e} = 0.5(\overline{u^2 + v^2 + w^2})$, $\bar{\theta}_v$ is a reference virtual potential temperature and ϵ is the molecular dissipation of TKE. The left-hand side term represents the tendency of TKE (TE), and the terms of the right-hand side are the shear production (S), the buoyancy production (B), the turbulent transport (T), the pressure transport (P) and the molecular dissipation term (D). The first two terms of the right-hand side are sources, the next two only redistribute the TKE vertically and the last one is a sink.

The total TKE budget for the B (pure buoyancy) and the BGS simulations after 8 hours of simulation are shown in Fig. 2. The different contributions are: the shear production (S), the buoyancy production (B), the turbulent transport (T), the pressure transport (P) and the molecular dissipation term (D). In the TKE budget of the B simulation (Fig. 2a), the primary source term is buoyancy. The dissipation term is constant with height except very close to the surface. With regard to the BGS TKE budget (Fig. 2b), the inclusion of the shear term affects the other terms of the budget, except the buoyancy term which, qualitatively, remains as it was in the B simulation. In order to balance the shear production term, the dissipation term increases its value and the pressure term becomes a consumption term at the inversion. Note that the shear production term is very small in mid-CBL. This is because a small amount of buoyancy forcing generates large thermals that can effectively mix the mean winds in mid-CBL reducing $\partial U/\partial z$ and hence reducing the shear production. In relation to the entrainment flux, it is relevant to notice the importance of the shear term as a production

term at the inversion. Consequently, we can expect an enhancement of this flux. In addition, current parameterizations of the entrainment flux should include the shear contribution (see next section).

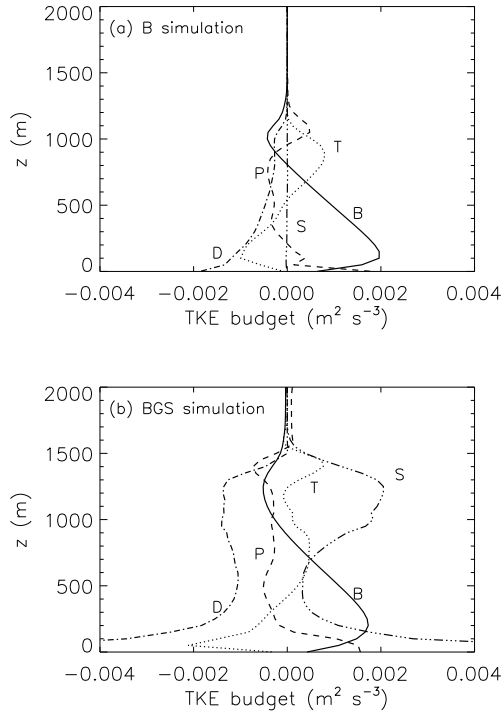


FIG. 2: Vertical distributions of the various terms (buoyancy, dissipation, pressure, transport and shear) in the TKE budget for (a) the B and (b) the BGS simulations after 8 hours of simulation (21 UTC).

3.3 Parameterization of the entrainment flux

Large atmospheric models are unable to calculate explicitly the entrainment flux and they describe it as a function of known quantities, such as the surface buoyancy flux or the friction velocity. To determine the contribution of the various mechanisms which drive the entrainment flux, it is convenient to parameterize the terms of the TKE equation by means of scaling. In this section, the value of $\beta = -\overline{w\theta_v}|_h / \overline{w\theta_v}|_0$ obtained from our LES runs is compared with some previous parameterizations based on slab models (see Tennekes and Driedonks 1981 for a review).

All the parameterizations presented here apply the entrainment formulation resulting from the local energy budget. Applying (1) at $z = h$ and parameterizing the terms using scaling arguments (Driedonks 1982), the entrainment ratio is written:

$$\beta = -\frac{\overline{w\theta_v}|_h}{\overline{w\theta_v}|_0} = C_F \left[1 + \eta^3 \left(\frac{u_*}{w_*} \right)^3 \right] \frac{1}{1 + C_T/Ri_t - C_M/Ri_{GS}}, \quad (2)$$

where u_* and w_* are the friction and convective velocities, respectively, and Ri_t and Ri_{GS} are two bulk Richardson numbers related to the temporal variation of the TKE and to the shear at the inversion zone:

$$Ri_t = \frac{gh}{\theta_v} \frac{\Delta\theta_v}{\sigma_w^2}, \quad Ri_{GS} = \frac{gh}{\theta_v} \frac{\Delta\theta_v}{(\Delta V_e)^2},$$

where h is the mixed-layer height, $\sigma_w^3 = w_*^3 + \eta^3 u_*^3$, $\overline{\theta_v}$ is a reference virtual potential temperature, $\Delta\theta_v$ is the jump of the virtual potential temperature across the inversion layer and ΔV_e is the module of the velocity jumps, ΔU and ΔV at the inversion base. C_F , η , C_T and C_M are constants which values for the different parameterizations are shown in table 1 (Tennekes 1973; Zilitinkevich 1975; André et al. 1978; Price et al. 1978; Driedonks 1982).

In Fig. 3, the β evolution during the central part of the day for the three simulations performed is shown. It is clear from the figure that, in general, wind shear in the boundary layer enhances the entrainment coefficient with respect the pure buoyancy case. Specifically, by comparing β for BG and BGS simulations one finds that, if the shear is not only at the surface level (BG simulation), but is also at the inversion (BGS simulation), the entrainment coefficient becomes larger. This figure also shows the evolution of the β parameter calculated from the expression (2) with the parameters shown in table 1. As is observed, a constant value $\beta \approx 0.2$ (expression 2 with $\eta = C_T = C_M = 0$) is a good parameterization for the B simulation. On the other hand, the parameterization BG slightly overestimates BG simulation. The BGS parameterization provides good description of the evolution of the β parameter only for the first two hours represented in Fig. 3. At the end of the day when convection decays, the factor $1/(1 - C_M/Ri_{GS})$ become very dominant and can double the β -ratio and then the parameterization will no longer fit the LES results.

	C_F	η	C_M	C_T
B	0.2	0	0	4
BG	0.2	2	0	4
BGS	0.2	2	0.7	4

Table 1: Parameters of expression (2) used for each of the comparisons.

Table 2 shows the mean values of the β parameter between 250 and 500 minutes of simulation (between 17:10 UTC and 21:20 UTC) for the different LES runs and for the parameterizations. Betts and Ball (1994) obtained from observations similar values to the BGS case ($\beta = 0.44 \pm 0.21$). As shown, the parameterization (2), which includes the relevant mechanisms for describing the entrainment processes, gives satisfactory results when the proposed constants are used.

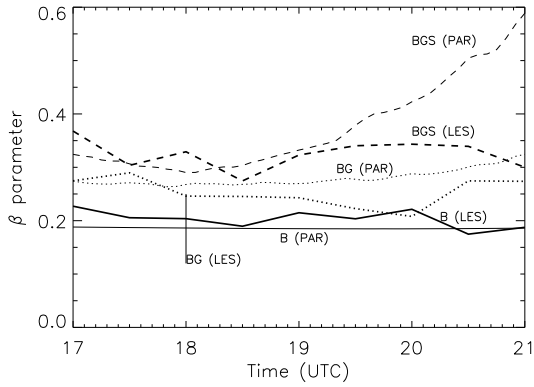


FIG. 3: Time evolution of the β parameter averaged every 30 minutes for the various LES runs (thick lines, LES) and provided by expression (2) (thin lines, PAR): B (solid line), BG (dotted line) and BGS (dashed line). The values of C_F , η , C_T and C_M in expression (2) for each of the comparisons are listed in Table 1.

	B	BG	BGS
LES	0.20	0.25	0.33
Parameterization ($C_T=0$)	0.2	0.31	0.46
Parameterization ($C_T=4$)	0.19	0.28	0.39

Table 2: Mean value (averaged between 17:10 UTC and 21:20 UTC) of the β parameter for LES results and the parameterization (2).

4. CONCLUSIONS

The influence of shear on the entrainment fluxes was studied by means of large-eddy simulations and observations. The results obtained in this paper show that LES can be used to describe the evolution of the boundary layer under realistic conditions. However, our main purpose was to analyze the role of shear in the entrainment processes. Therefore, two additional simulations, one without shear and one with shear only at the surface, were carried out. From the results, it is clear that the presence of horizontal geostrophic winds in convective situations increases the entrainment flux and modifies the convection pattern. Moreover, the entrainment flux can be further enhanced if shear is present not only at the surface but also in the inversion zone.

By means of the LES, it is possible to obtain the TKE budget. This is a crucial point because the influence of shear at the inversion is clearly shown in the vertical distribution of the various terms of the TKE budget. The TKE budget of the BGS simulation shows that shear is the largest term in the entrainment zone, and it is therefore necessary to take it into account in the parameterization of the TKE budget. From the TKE budget and by comparing previous parameterizations of the entrainment flux used in large-scale models with the LES results, an expression for the ratio of entrainment flux to the surface flux (β) is proposed. This expression that fits quite well with the LES results can be used in general circulation

models.

Acknowledgements

The data used were obtained from the Atmospheric Radiation Measurement (ARM) Program sponsored by the U.S. Department of Energy. We are specially grateful to Thomas Ackerman, David Cook, Mark Miller and Ping Zhu for supplying and interpreting the data. We thank Mandy Khaiyer of AS&M, Inc., Hampton, Virginia for providing the GOES imagery. Discussions with Harm Jonker were also greatly appreciated. D. Pino was partially supported by the project IMPACTE (CIRIT, DME, Barcelona, Spain). Part of the visits by the first author to the IMAU were supported by the EU program EUROCS (European Project on Cloud Systems In Climate Models). The resources of CESCA and CEPBA were used for parts of the work.

REFERENCES

- André, J. C., de Moor, G., Lacarrère, P., Therry, G. and du Vachat, R., 1978: Modeling the 24-hr Evolution of the Mean and Turbulent Structure of the Planetary Boundary Layer, *J. Atmos. Sci.* **35**, 1861–1883.
- Betts, A. K. and Ball J. H., 1994: Budget Analysis of FIFE 1987 Sonde Data, *J. Geophys. Res.* **99**, 3655–3666.
- Christian, T. W. and Wakimoto, R. M., 1989: The Relationship between Radar Reflectivities and Clouds Associated with Horizontal Roll Convection on 8 August 1982, *Mon. Wea. Rev.* **117**, 1530–1544.
- Cuijpers, J. W. M. and Duynkerke, P. G., 1993: Large Eddy Simulation of Trade Wind Cumulus Clouds, *J. Atmos. Sci.* **50**, 3894–3908.
- Cuijpers, J. W. M. and Holtslag, A. A. M., 1998: Impact of Skewness and Nonlocal Effect on Scalar and Buoyancy Fluxes in Convective Boundary Layers, *J. Atmos. Sci.* **55**, 151–162.
- Driedonks, A. G. M., 1982: Models and Observations of the Growth of the Atmospheric Boundary Layer, *Bound.-Layer Meteor.* **23**, 283–306.
- Price, J. F., Mooers, C. N. K. and van Leer, J. C., 1978: Observation and Simulation of Storm-Induced Mixed Layer Deepening, *J. Phys. Oceanogr.* **8**, 582–599.
- Schmidt, H. and Schumann, U., 1989: Coherent Structure of the Convective Boundary Layer Derived from Large-Eddy Simulations, *J. Fluid Mech.* **200**, 511–562.
- Tennekes, H., 1973: A Model for the Dynamics of the Inversion above a Convective Boundary Layer, *J. Atmos. Sci.* **30**, 558–567.
- Tennekes, and Driedonks, A. G. M., 1981: Basic Entrainment Equations for the Atmospheric Boundary Layer, *Bound.-Layer Meteor.* **20**, 515–531.
- Zilitinkevich, S. S., 1975: Comments on a Paper by H. Tennekes, *J. Atmos. Sci.* **32**, 991–995.